Journal of the Meteorological Society of Japan, Vol. 72, No. 6, pp. 937–957, 1994

Trends and Decadal-Scale Fluctuations of Surface Air Temperature and Precipitation over China and Mongolia during the Recent 40 Year Period (1951–1990)

By Akiyo Yatagai and Tetsuzo Yasunari

Institute of Geoscience, University of Tsukuba, Ibaraki 305, Japan

(Manuscript received 27 December 1993, in revised form 7 October 1994)

Abstract

The time-space structures of long-term trends and the decadal-scale variations of seasonal temperature and precipitation over China and Mongolia are investigated by using the 5-year moving averaged data from 1951 to 1990. An empirical orthogonal function (EOF) technique is applied to seasonal temperature and precipitation. The changes of atmospheric circulation patterns with these trends, and long-term fluctuations are deduced by using 500 hPa height and surface pressure fields. The correspondence of these components with the Northern Hemispheric surface air temperature (NHT) is examined.

The increasing linear trend in the annual mean temperature is remarkable, especially in the northern part of China and Mongolia, while the decreasing trend is conspicuous in the area from Sichuan to Yunnan Province. The increasing trend in the annual mean temperature is due mostly to the anomalies in winter and spring. These trends in winter temperature are directly related to the decadal-scale change of the locations of Siberian High and mid-tropospheric trough over Eurasia, and are associated with the hemispheric circulation changes.

The annual precipitation, in contrast, does not show a clear linear trend over the whole of China except in the southern part of China, where a significant increasing trend is noted. Summer precipitation shows a remarkable decadal-scale fluctuation in the first two dominant EOF modes. The first EOF represents the increasing trend in the middle and northwest part of China, while the second EOF represents the oscillation between the southern part of China and the rest of the country, which is closely related to the summertime NHT.

1. Introduction

Recently, global or hemispheric-scale climatic variations have become a matter of great concern, particularly associated with the "global warming" issue. IPCC (1990,1992) concluded that the global-mean surface air temperature has increased by 0.3°C to 0.6°C over the last 100 years. They summarized that there is a natural greenhouse effect which already keeps the Earth warmer than it would otherwise be, however, it is still not possible to attribute, with high confidence, all or even a large part of the observed global warming to the enhanced greenhouse effect. Actually, the global-averaged surface air temperature has not increased constantly, as the concentration of greenhouse gases (*e.g.*, carbon dioxide) has. The global-averaged surface air temperature shows some decadal-scale variation rather than a constant increase, even after removing short-term (less than a few years) oscillation. Recently Nitta and Yoshimura (1993) examined inter-decadal temperature variations for the near-global and regional-scale domains. They showed that the temperature has inter-decadal variabilities, with the largest warming for the recent 20 years, but with a cooling trend during 1940–1970. However, the associations of these global or hemispheric temperature trends and decadal-scale oscillation with regional climate change are still not clear. Bradley *et al.* (1987) showed that the time series of seasonal mean surface air temperature averaged over China is highly correlated with the hemispheric-mean temperature, especially in the long-term variation, though time-space characteristics of seasonal temperature fluctuation were not considered in their paper.

There have been, so far, a considerable number of studies of the inter-annual climatic variations in China, particularly associated with the El Niño/Southern Oscillation (ENSO). However, few

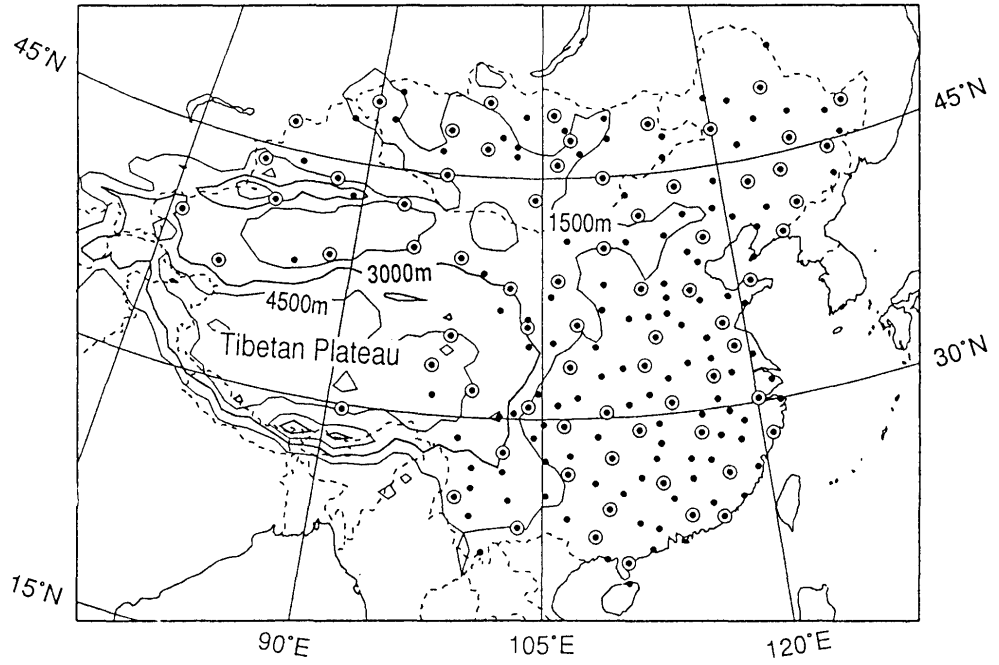

Fig. 1. Geographical distribution of the observation stations. Dots show all 185 stations, and large circles are the selected 71 stations for EOF analysis. Note Tooroi (44.93°N, 96.77°E) is missing in precipitation data.

studies have been devoted to the decadal-scale variations in China during the recent several decades. The studies by Li *et al.* (1990), Chen *et al.* (1991), Chen *et al.* (1992) and Huang (1992) have shown some different spatial patterns for each decade. Chen *et al.* (1991), for example, reported the precipitation in the most parts of China has decreased, especially in North and Northwest China, where a serious desertification has been progressing. Since the precipitation decrease must be one of the cause of desertification, it is necessary to evaluate the trend and decadal-scale fluctuations over a broader area including the adjacent countries. Identifying these fluctuations and their relations to large-scale atmospheric circulation is essential for a better understanding of the mechanism of desertification.

This study aims to examine the time-space structures of the long-term linear trend and the decadal-scale fluctuations of seasonal mean temperature and precipitation over China and Mongolia and the inter-relation between these two climatic variables. The atmospheric circulation patterns associated with these fluctuations are also discussed. The relation between some major patterns recognized in temperature and precipitation fields and the Northern Hemispheric surface air temperature (NHT) is additionally described.

The linear trends of annual and seasonal mean temperature and precipitation are described in Section 3. The decadal-scale fluctuations of temperature which derived from the empirical orthogonal function (EOF) analysis and their relations to the atmospheric circulation and NHT are discussed in Section 4. A similar analysis for precipitation is presented in Section 5. A summary with concluding remarks follows in Section 6.

2. Data and method of analysis

The main data set for this study comprises the monthly precipitation and mean temperature data of 160 stations in China (compiled by the State Meteorological Administration of China) and 25 stations (23 stations for precipitation) in Mongolia. The locations of the stations are shown in Fig. 1. These data cover 40 years, from 1951 to 1990, although 26 stations' data are from 1953 or 1954. Seasonal data are rearranged by averaging (temperature) or summing (precipitation) the data of three months of each season (*e.g.*, DJF, MAM, JJA and SON).

First of all, we fitted a linear trend to annual or seasonal temperature and precipitation data and tested their statistical significance. Secondly, to examine the time-space structure of the decadal-scale variation of temperature and precipitation, the empirical orthogonal function (EOF) analysis is applied to the 5-year moving averaged seasonal time series. Since the 185 stations shown in dots in Fig. 1 are not distributed uniformly, the 71 stations, which are available from 1951, are selected to deduce the dominant spatial pattern in applying EOF analysis (large circles in Fig. 1).

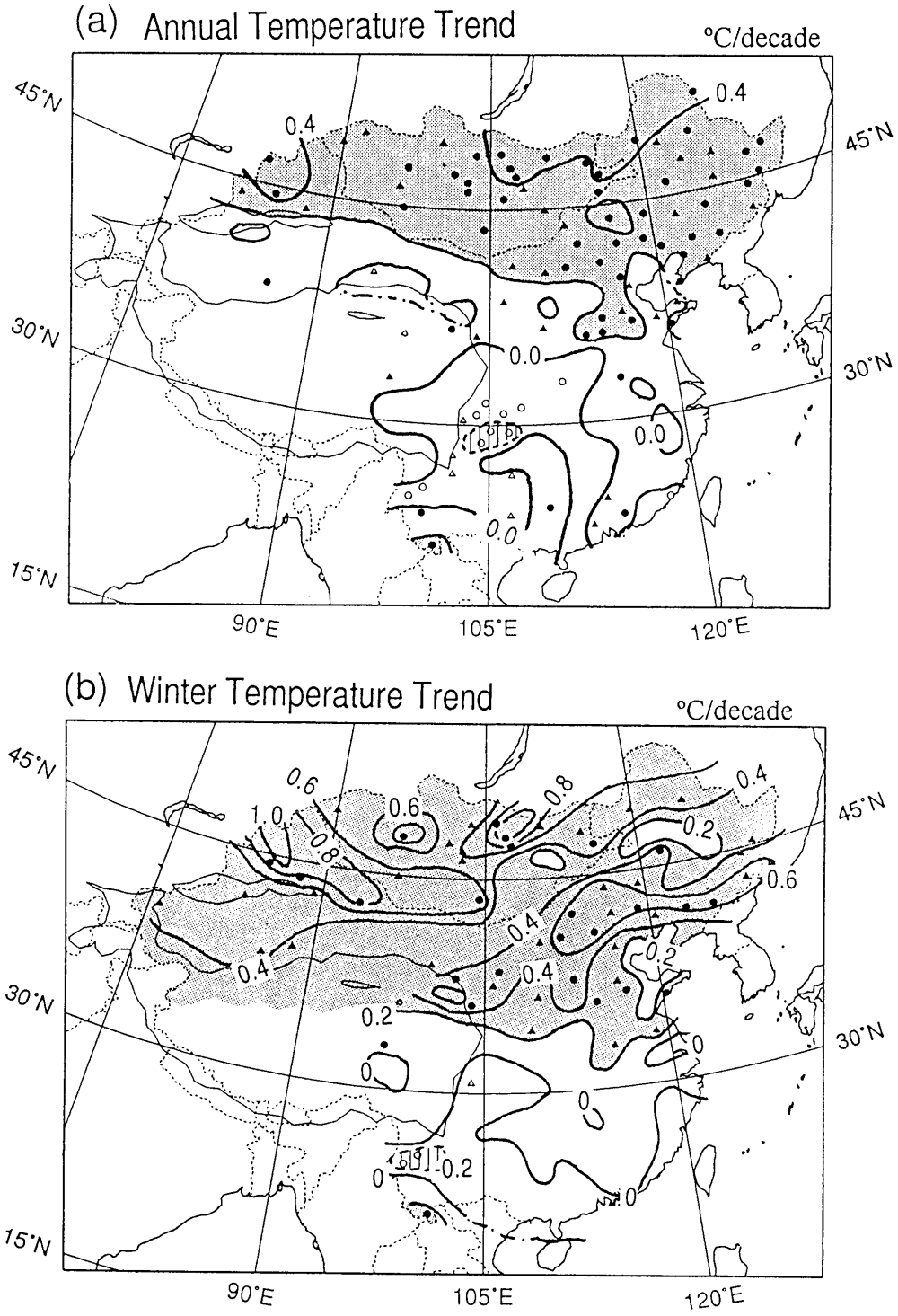

Fig. 2. Linear trend of (a) annual, (b) winter, (c) spring and (d) summer mean surface air temperatures in 1951–1990 (°C/decade). Shaded and hatched area show temperature warming more than 0.2°C/decade and cooling less than −0.2°C/decade, respectively. Black and open circles are significant at the 1 % level, while triangles are the same of 5 % level. Contours are every 0.2°C/decade, with cooling region (negative values) are shown with dashed lines and open marks.

The monthly mean sea level pressure (SLP) and 500 hPa geopotential height on a 10°longitude/latitude grid in the Northern Hemisphere, compiled by the Japan Meteorological Agency, are used to examine the atmospheric circulation field. 5-year moving averaged seasonal anomalies are computed from these data sets, with which up to decadal-scale atmospheric circulation patterns are

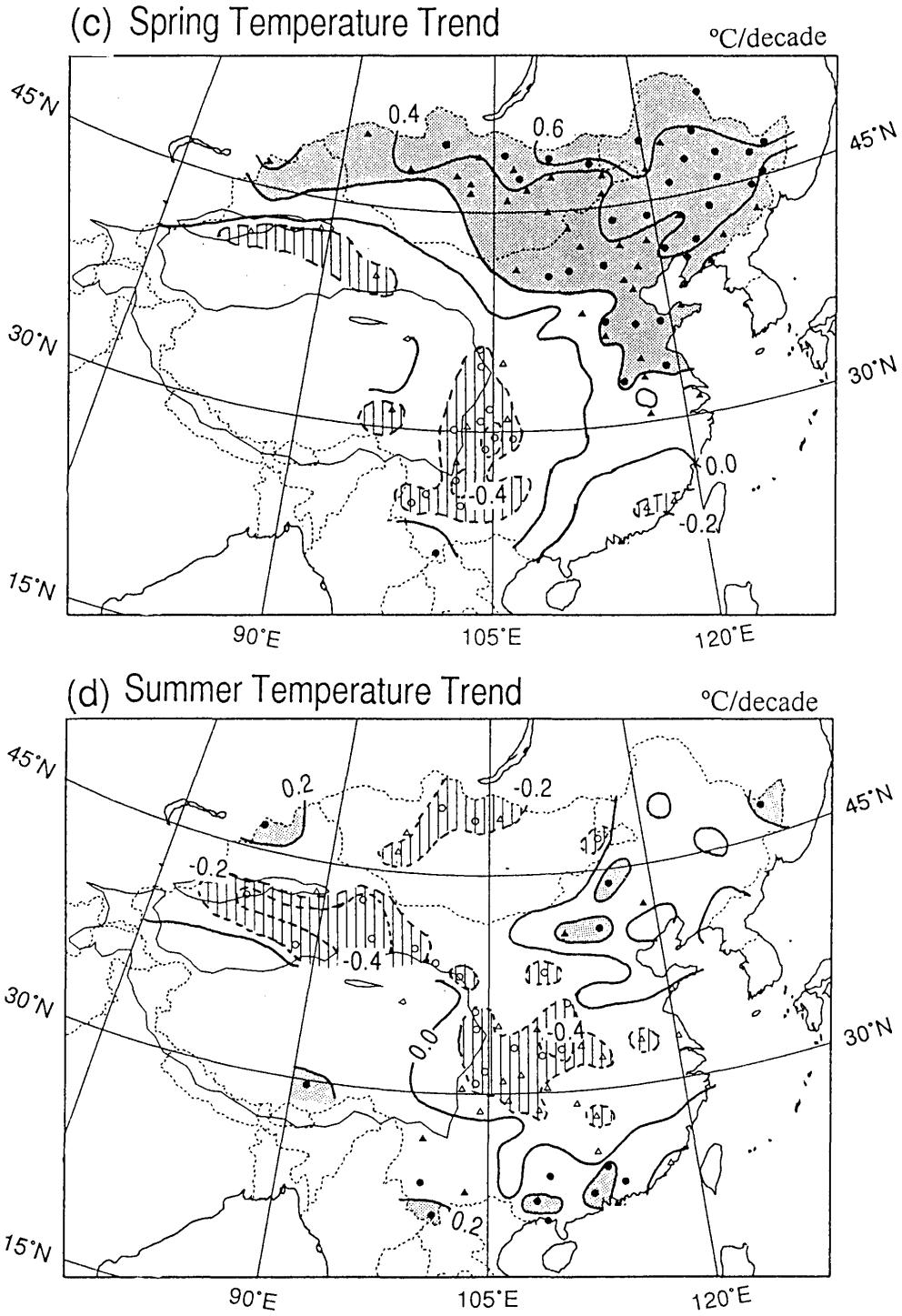

Fig. 2. (Continued)

constructed to compare with the decadal-scale components of temperature and precipitation.

The Northern Hemispheric land-based surface mean air temperature data set (hereafter referred to as NHT) adopted from Jones *et al.* (1986) and updated to 1990 is also used. These data are also arranged into 5-year moving averaged seasonal anomaly data.

3. Linear trends of annual and seasonal mean temperature and precipitation

3.1 Temperature

Figure 2a shows the distribution of linear trend in the annual mean temperature from 1951 to 1990. Many stations except Central China show remarkable trends exceeding significant levels. An increasing trend is notable, especially in Mongolia,

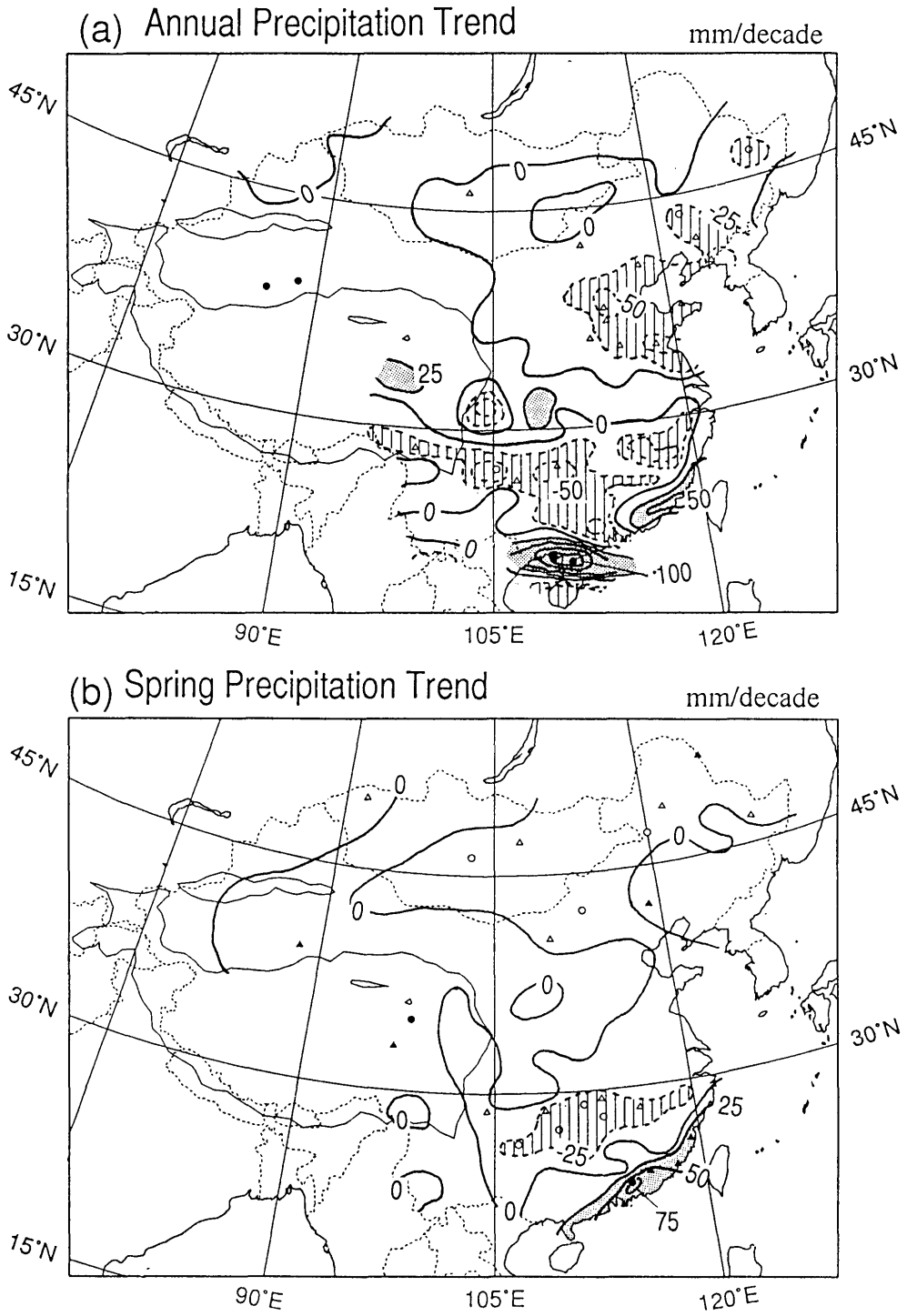

Fig. 3. Linear trend of (a) annual, (b) spring and (c) summer precipitations over the period 1951–1990. Shaded (hatched) area shows precipitation increasing (decreasing) more (less) than 25 mm/decade (−25 mm/decade). The contour interval is 25 mm/decade with negative anomalies dashed. Others are the same as Fig. 2.

Northeast China and Nei Mongol (0.4°C/decade), whereas a decreasing trend is conspicuous in Southwest China (−0.2°C/decade). This pattern over China is consistent with the distribution of annual mean temperature difference between the 1980s and the 1950s over China (*e.g.*, Li *et al.*, 1990; Chen *et al.*, 1991, 1992). The remarkable warming trend pattern extends from Northeast and Northwest China, which seems to be a part of the warming area in the recent decade (1980s) centered over the north-

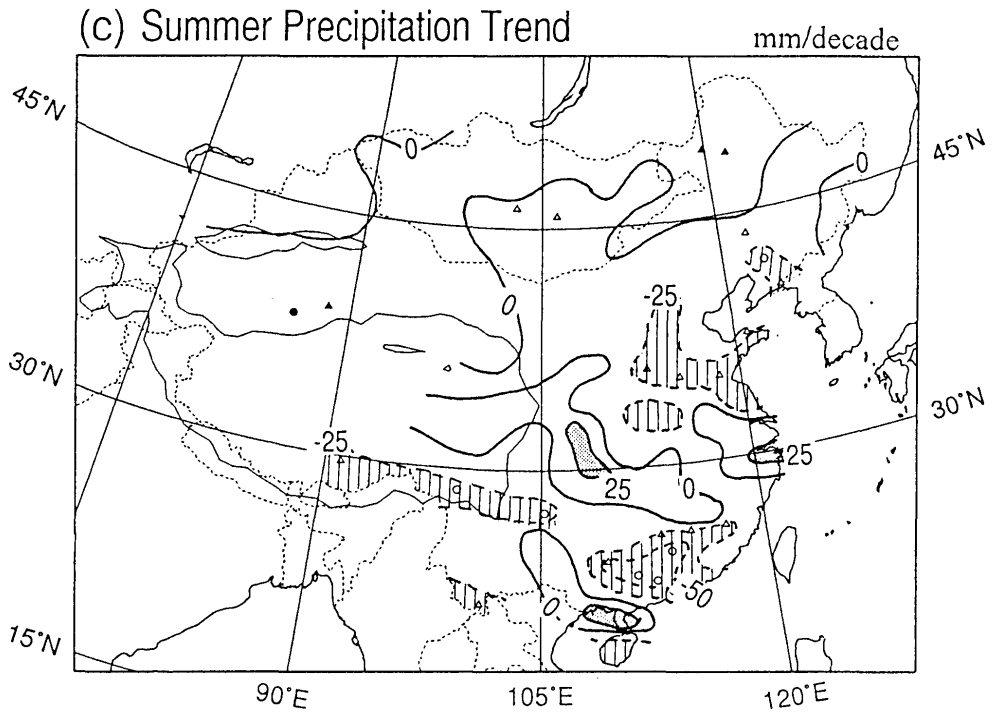

Fig. 3. (Continued)

ern and central Eurasia (IPCC, 1990, 1992; Jones and Briffa, 1992).

Figure 2b depicts the linear trend of temperature in winter. The spatial pattern is similar to that of the annual mean temperature (Fig. 2a), but shows a little more complicated feature with large values, especially in Northwest China and Mongolia. The largest increasing trend is apparent to the north of Tianshan Mountains and northeast part of Mongolia with the value exceeding 0.8°C/decade. Most of the stations indicate significant increasing trend to the north of 35°N, while South and Southwest China exhibit decreasing trends, which do not exceed significant levels, except in the northern part of Yunnan Province.

In spring (Fig. 2c), the overall pattern resembles those of the annual mean (Fig. 2a) and winter (Fig. 2b). In winter, the boundary between the cooling and the warming areas lies zonally along 35°N, but in spring it lies from NW to SE. Namely, clear warming trends are seen over Mongolia, North, Northeast China and the northeast part of Central China (Anhui and Jiangsu Province), while large significant cooling trends are seen around the periphery of the Tibetan Plateau (the south part of Xinjiang, Gansu, Shaanxi, Sichuan and Yunnan Provinces). The coastal area of South China (Fujian) also shows cooling trends. The largest increasing trend is observed in Northeast China with the value exceeding 0.6°C/decade. The large decreasing trends over Sichuan and Yunnan seem to be responsible for the same trend in the annual mean trend (Fig. 2a). The warming trend is weak to the north of Tianshan Mountains and a weak cooling trend is seen in the Tarim Basin.

In the summer season (Fig. 2d), the spatial pattern of trend is quite different from those of the annual mean and winter. A decreasing trend is significant in the extended area from the Tarim Basin to Central China and parts of Mongolia. In other areas — to the north and the south of this area — warming trends are seen, though these are not obvious, except in South China. The distribution pattern of summer temperature trends is consistent with that of difference between the 1980s and 1950s, as shown by Chen *et al.* (1991).

The linear trends are generally not clear in autumn (not shown). Significant increasing trends are seen in Mongolia and North China, whereas a weak decreasing trend is located at nearly the same region as for the annual temperature.

The remarkable increasing trends to the north of 40°N, especially in the annual mean, winter and spring, are generally consistent with the results from the hemispheric data (*e.g.*, IPCC, 1990, 1992; Jones and Briffa, 1992). The remarkable warming trend over China and Mongolia in winter and spring as presented here contributes partly to the hemispheric warming in recent years.

3.2 Precipitation

Figure 3a shows the linear trend of annual precipitation over China and Mongolia. The overall pattern is more complicated and less significant than that of

the temperature field. An large increasing trend is found in South China, particularly over the Leizhou Peninsula, while a narrow belt of an increasing trend is seen in the middle Yangtze River Basin. The arid region to the north of the Tibetan Plateau shows some increasing trend, though it is not statistically significant. Other regions generally show a decreasing trend with the centers in North China and in Southwest China. The overall pattern is consistent with the pattern of the annual precipitation difference between 1980s and 1950s, deduced by Chen *et al.* (1991, 1992).

In most parts of China and Mongolia, precipitation is dominant in summer. However, in the southeast part of China precipitation is prevalent more in spring than in summer, and, in Northwest China, the proportion of spring precipitation is comparable to that of summer (Yoshino and Chiba, 1984). In any case, since the total of spring and summer precipitation accounts for more than 70 % of the annual total in all parts of China and Mongolia, we will focus only on the summer and spring precipitation trends.

In spring (Fig. 3b), a remarkable increasing trend is noted in the coastal area of South China, whereas a significant decreasing trend dominateds in the middle and lower Yangtze Basin (Hunan, Jianxi and Zhejiang Province). Since most of precipitation takes place in spring in these areas, the annual precipitation is basically controlled by the features in spring. The coupled pattern of increase in the South and decrease in the southern part of Central China is likely to be related to the temperature trends (Fig. 2c), which show a clear cooling trend in the South and weak warming around Hunan, Jianxi and Zhejiang. This precipitation is likely to be related to the change in the seasonal march of the Meiyu Frontal Zone (*i.e.*, seasonal delay or less northward migration), which has brought more rain to South China in recent years. These trends in South China exert the same trend on the annual precipitation trend. Mongolia does not have so much precipitation in spring, but some stations show a significant decreasing trend.

The pattern of precipitation trend in summer (Fig. 3c) resembles, as a whole, that of the annual pattern (Fig. 3a). This pattern is generally negatively correlated with that of the temperature trend in the same season, though the decreasing (increasing) precipitation (temperature) trend over Yangtze River distributes more narrowly (widely). Some previous studies have already noted significant negative correlation between temperature and precipitation in most part of China (Huang, 1991; Wang and Zhang, 1992). Wang and Zhang (1992), for example, pointed out that the correlation between the temperature and number of precipitation days in Beijing in summer is presumably due to two factors: (1) the cloudy sky in a rainy day reduces direct solar radiation; and (2) the continuous rain is often caused by the invasion of cold air masses. Another possibility may be that much more evaporation after precipitation causes the cooling by suppressing sensible heat flux at the surface. Further investigation should be made of the relation between precipitation and temperature.

A significant trend is noted in one region from Southwest China to South China, and another in Northeast China which contain statistically significant stations. Increasing trends are widely distributed from the Taklimakan Desert to the middle and lower parts of the Yangtze River. It is worthwhile to note that the arid and semi-arid region to the east of 105°E generally exhibits a decreasing trend in North China and Mongolia. The Leizhou Peninsula shows an increasing trend, though not significant.

4. Principal EOF modes of temperature and circulation in winter

In order to examine the time-space structure of the decadal-scale fluctuations, we applied the EOF analysis to the 5-year moving averaged seasonal temperature anomalies. Since the annual mean temperature trend is largely affected by those of winter and spring, as is shown in Section 3, we will focus only on the winter temperature. The major EOFs are also correlated to 500 hPa height, SLP anomalies, and NHTs.

4.1 Principal modes of temperature in winter

A correlation matrix is used for computing the eigenvalues and eigenvectors of EOFs. The variances and cumulative variances of the first five EOFs for winter temperature anomalies are presented in Table 1. Since the first two components explain 66.3 % of the total variances, we feature these two components. The spatial patterns and time coefficients of the first two EOFs have been plotted in Fig. 4.

The first EOF shares more than 50 % of the total variance, which represents the major temperature fluctuation over China and Mongolia. This spatial pattern (Fig. 4a) represents the simultaneous temperature fluctuation over most part of the analysis area, except the Tibetan Plateau and Southwest

Table 1. The variances and cumulative variances of the first five EOFs of winter temperature.

Component	1	2	3	4	5
Variance (%)	51.3	15.0	9.2	6.8	6.4
Cumulative Variance (%)	51.3	66.3	75.5	82.3	88.7

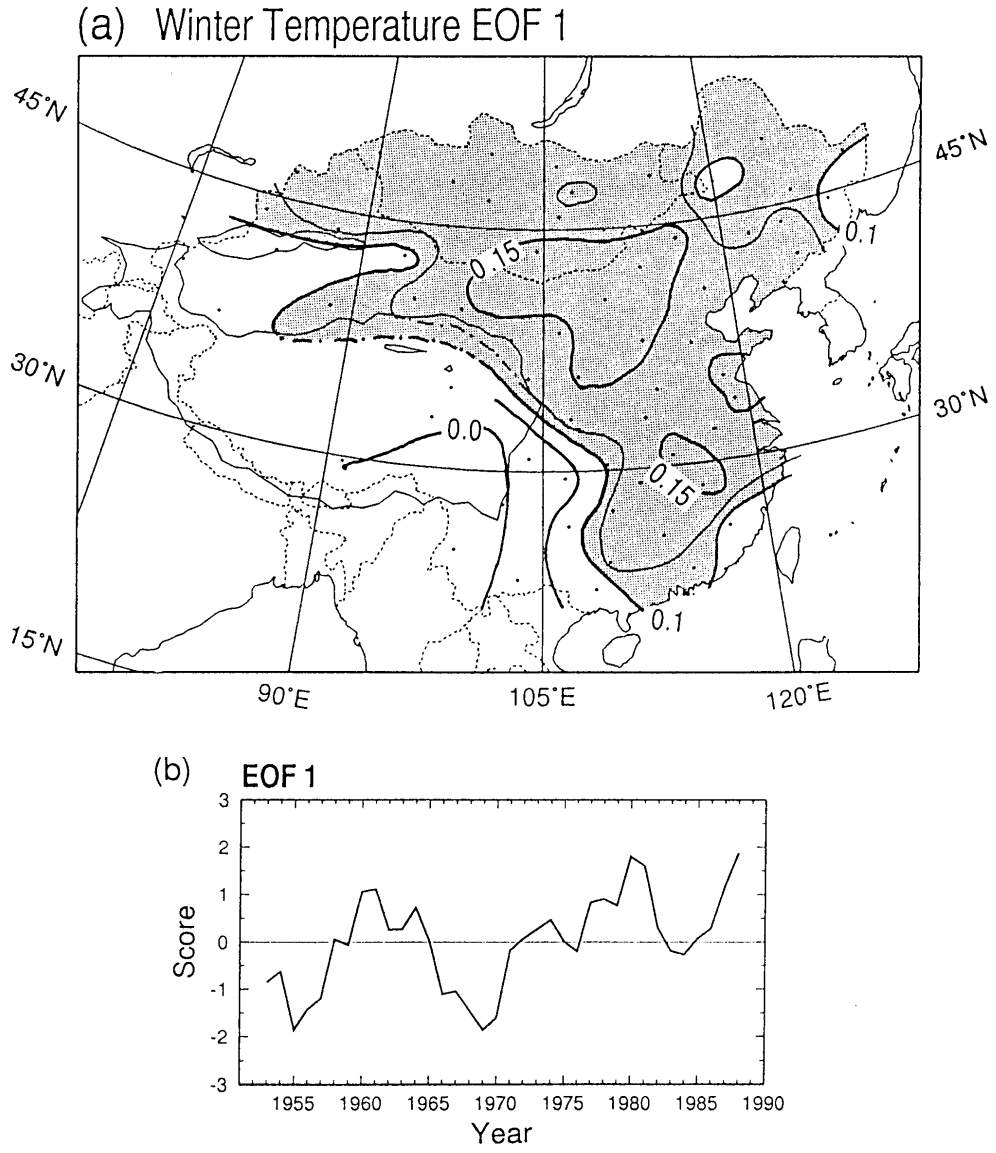

Fig. 4. Eigenvector patterns and time coefficients of the first two EOFs of winter temperature. (a) (b) the 1st component, (c) (d) the 2nd component. (a) Dots show the 71 stations applied to the EOF analysis. Shaded area indicates the eigenvector exceeds 0.1. The contour interval is 0.05, but the 0.125 contour is also drawn additionally by thin line. (b) Scores are standardized. (c) Same as (a), but the contour interval is 0.1 with negative anomalies dashed. The hatched area shows the negative eigenvector below −0.1.

China. The time sequence of the coefficient (Fig. 4b) shows a decadal-scale periodic fluctuation with the two peaks in the beginning of the 1960s, the beginning of the 1980s, and with a maximum in the late 1980s. A slightly increasing linear trend is also discernible.

The same figures, but for the second component, are mapped in Fig. 4c and 4d. The second component accounts for 15 % of the total variance. This pattern represents a dipole-like oscillation; South and Southwest China have high positive eigenvectors while Northwest, Northeast China and Mongolia show high negative values. This dipole pattern corresponds to that of the linear trend of change in winter temperature (Fig. 2a), yet eigenvectors are very high over South and Southwest China and not so high around Central China and Nei Mongol. So we can say though the variance of EOF 2 is much smaller than EOF 1, it is very important to recent decadal scale oscillation of East Asia. In fact, the score of EOF 2 shows a large decrease in the first several years (mid 1950s) and early 1980s, while the long term variation in 1960s and 1970s is relatively small. As the anomalies of the first and last decade are essential to the decadal-scale of this mode, the linear trend pattern (Fig. 2b) corresponds well with

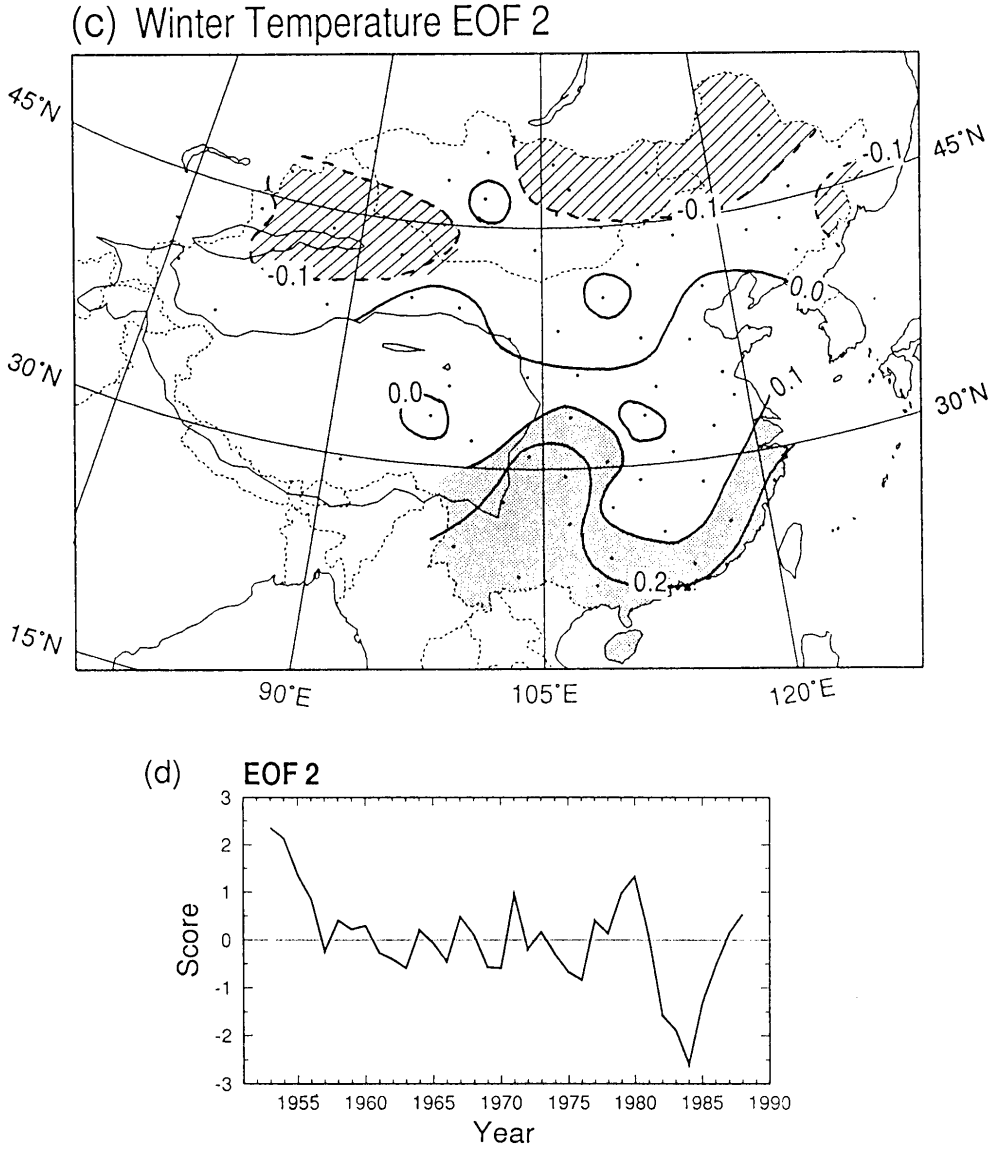

Fig. 4. (Continued)

that of the winter temperature difference between the 1980s and 1950s of the previous studies (Li *et al.*, 1990; Chen *et al.*, 1991, 1992).

These two modes seem to be closely related to the patterns of cold-wave propagation over China, discussed by Yasunari and Tian (1990). They calculated EOFs for the monthly mean surface temperature anomaly for the winter months of a 28 year period (1959–1986) to investigate the dominant time-space structure of cold surges affecting Yunnan Province and the whole of China. Interestingly, two dominant eigenvectors derived here show similar patterns for the monthly temperature in winter described in their paper. The original data sets used in their study are basically the same in China, except for the period. They pointed out that the second component used in their analysis, which is basically same as our second component, represents the mode of cold surges dominantly affecting the whole Yunnan Province, and called it the Yunnan-mode. Their first component is related to the temperature anomaly over the whole of the Chinese Plain, and is called the Plain mode. It is therefore conjectured that the two modes drawn out here represent the decadal-scale changes of the cold surge intrusion patterns over China, which in turn strongly affect the winter temperature patterns over China.

4.2 Atmospheric circulation patterns associated with the winter temperature EOFs

The atmospheric circulation patterns related to the above two major modes of winter temperature are presented by computing the no-lag correlation coefficients between the time coefficients of the EOFs and the 500 hPa height and SLP anomalies of the corresponding season over the Northern

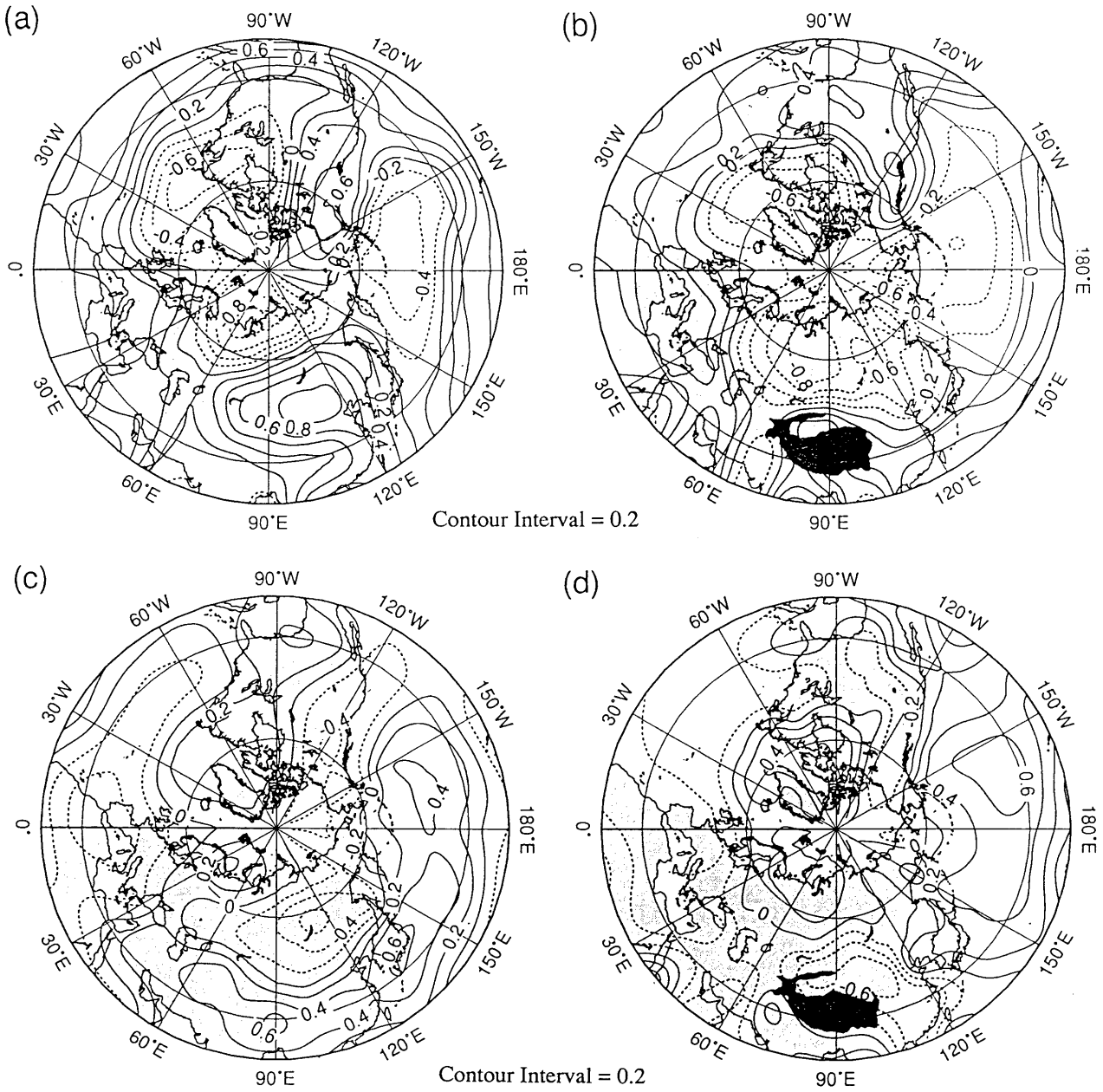

Fig. 5. Correlation coefficients between time coefficient of the first component and (a) the 500 hPa height and (b) SLP anomalies in winter temperature. The contour interval is 0.2 with negative values dashed. (c) (d) are same as (a) (b), but for the second component.

Hemisphere. The correlation patterns between each component and the 500 hPa height or SLP have been mapped in Fig. 5 ((a) EOF 1 and the 500 hPa height and (b) EOF 1 and SLP (c) EOF 2 and the 500 hPa height (d) EOF 2 and SLP).

In Fig. 5a, a strong dipole pattern can be seen over the Eurasian Continent, which was labeled as the NA (Northern Asian) pattern by Barnstern and Livezey (1987), and the ANA (Arctic and North Asia) pattern by Yasunari and Seki (1992). This pattern suggests that when the first component of winter temperature anomaly is positive, the height anomaly over the northern periphery of the continent is negative, and that around Mongolia and the northern part of China is positive. This mode explains that when the winter temperature over the most part of China and Mongolia is relatively high, the pressure gradient over Siberia (40–60°N) is relatively large and the strong upper westerly jet prevails to the north of China (high index-type circulation). In this case, the negative area around 60°E over central Asia extends southward, which implies that the trough there is relatively strong when the temperature of whole of study area is warm. An-

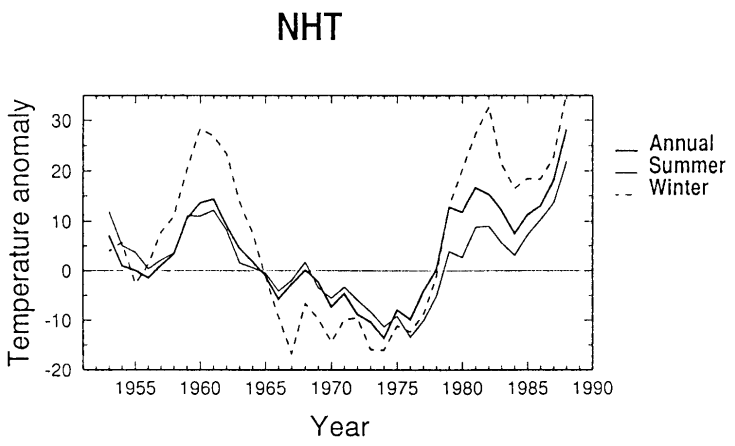

Fig. 6. Northern Hemispheric annual, winter and summer mean air temperatures. 5-year running meaned to the Jones original datasets. Thick and thin lines are annual and summer series, and dashed line for winter.

other notable feature is seen from the Pacific Ocean to the Atlantic through North America, which has been called the Pacific/North American (PNA) pattern (Wallace and Gutzler, 1981).

The correlation pattern with SLP (Fig. 5b) is similar to that of the 500 hPa anomalies, but no distinct positive correlation is apparent over and around Mongolia. The large negative correlation coefficient is noticeable over central Siberia, which suggests that the SLP is relatively low (the Siberian high is relatively weak) when the temperature in the whole of China and Mongolia is relatively high. The total feature over the North Atlantic Ocean and the northwestern part of North America is similar to that of the 500 hPa (Fig. 5a).

These two correlation patterns suggest that the first component of winter temperature over China is directly linked to the hemispheric circulation change with the high (or low) index atmospheric circulation over the whole of the Eurasian Continent combined with low (or high) index over the Atlantic and North America including the change of PNA pattern. The correlation patterns at 500 hPa and SLP suggests that the anomaly circulation field over Eurasia (ANA pattern) has a baroclinic structure, while barotropic structure is fundamental for the North America/North Pacific (PNA pattern).

In contrast, the second component is more strongly associated with the change of the regional circulation pattern over East Asia through the Pacific sector (Fig. 5c and 5d). The high correlation, either positive or negative, are distributed both at the 500 hPa and SLP fields mainly over Eurasia and the North Pacific. Over the Eurasian Continent, at 500 hPa (Fig. 5c) a center of significant negative correlation is located over Lake Baikal, which implies that the geopotential height there has been becoming higher in recent years. As for the SLP correlation pattern (Fig. 5d), the negative correlation is dominant along the northern and eastern peripheries of the Tibetan Plateau, which suggests that the cold air intrusion in this area has intensified locally in the recent years, and as a result it has become colder in South and Southwest China. This result is consistent with Fig. 2b and Fig. 4c, showing the cooling trend in the South and Southwest China in recent years.

Recently, strong intensification of the Aleutian lows during 1977–1986 (1977–1988) has been noted (Kashiwabara, 1987; Trenberth, 1990 *etc.*) as part of the decadal-scale variations or "climatic jump" in winter. Nitta and Yamada (1989) noted that the polarity of the PNA pattern during winter has changed considerably between the period of 1977–86 and 1967–76, and that this change may be associated with tropical heat sources enhanced by the recent warming of the tropical SSTs.

The High negative/positive correlation seen over the Pacific Ocean to the north of 30°N in Fig. 5a–5d does not contradict with the recent lowering trend of Alleutian low and polarity change. However, the timing of changing signal of the two modes deduced here are not consistent timing with the abrupt change in 1977.

4.3 Relationship of the two modes to the hemispheric temperature

To investigate the relationship between the two major components of winter temperature EOFs over China and the hemispheric winter temperature change, the simultaneous correlation is computed between the first two winter temperature EOFs and the 5-year moving averaged NHT for the period of 1953–1988. The time series of NHT of annual, winter and summer are shown in Fig. 6. The standard deviation of NHT is the greatest in winter and the least in summer. While, taking the correla-

tions between the annual NHT and monthly NHT, the correlations are the greatest during the summer months and weak in winter (Jones and Briffa, 1992). The correlation between the first component deduced here and the wintertime NHT are stronger than that of the second component (0.57 and −0.14, respectively). The three maximum of EOF 1 match with that of NHT winter. However tendency is different in 1965–1978. The strong warming trend of the northern part of this study area in winter (and spring) affect the annual trend pattern as shown in subsection 3.2, however, the dominant decadal-scale modes of study area does not show a high correlation with winter NHT.

5. Principal EOF modes of precipitation, temperature and circulation in summer

As we have elucidated, the variation of summer precipitation contributes most to that of the annual precipitation. We, therefore, focus on the time-space structure of decadal-scale variation in the summer precipitation. In order to examine the relationship between the principal modes of summer precipitation and that of summer temperature, we also applied EOF analysis to the temperature in summer. Therefore we can compare the dominant modes of temperature and precipitation in summer over China and Mongolia with the summertime NHT. Atmospheric circulation patterns associated with these fluctuation are also discussed.

5.1 Principal modes of precipitation in summer

The variance of leading EOFs derived from summer precipitation is listed in Table 2. The proportion of the major components of summer precipitation are not so large as those of winter temperature. Figure 7 shows (a) the eigenvector pattern and (b) time coefficients of the first component, and (c) (d) similarly for the second component. The first EOF pattern appears to be similar to that of the linear trend (Fig. 3c). The trend pattern was emphasized over the area of large precipitation. However, the eigenvector pattern represents well the spatial variation of the anomaly, even in arid and semi-arid regions, by utilizing correlation matrix and the uniformly located variables (stations) shown by dots in Fig. 7a. A large negative area is dominant in Northwest and Central China. Two positive areas are seen in Mongolia to North China, and South and Southwest China. Taking account of the time coefficients (Fig. 7b), these positive (negative) areas correspond to the areas where the summer precipitation shows a decreasing (increasing) trend. The time series (Fig. 7b) generally shows, in fact, a decreasing trend, with a maximum and a minimum around 1960 and 1982, respectively. The decadal-scale periodic oscillation of this mode seems to be vague in this time series.

Table 2. The variances and cumulative variances of the first five EOFs of summer precipitation.

Component	1	2	3	4	5
Variance (%)	21.3	17.8	13.7	9.7	8.3
Cumulative Variance (%)	21.3	39.1	52.8	62.5	70.8

In the arid and semi-arid region of China, a contrasting eigenvector opposite pattern with negative (positive) to the west (east) of 105°E is noticeable. The polarity in Northwest China (around Taklimakan Desert) is of the same phase as that of Central China (Yangtze River Basin), whereas the variation in Nei Mongol and North China is of the same phase as that of Mongolia and South and Southwest China.

This spatial pattern closely resembles one of the figures of Wang and Zhao (1981), which was derived from summer precipitation EOF analysis using non-filtered instrumental data (1951–1974). This three-belt eigenvector (according to Wang and Zhao, 1981) is also deduced from the historical drought/flood data from 1450, though it covers the east of 100°E. The three-belt pattern over eastern part of China was also found in Tian and Yasunari (1992), though the pattern is different to the west of 105°E. They applied EOF analysis to 2–4 year period summer rainfall (May to September) series. The filtering period of their and our analysis are completely different and the months calculating summer precipitation are also different. However it is safely to say that this three belt pattern is very common in the summer precipitation variation.

Figures 7c and 7d show the eigenvector pattern and time coefficients of the second component, respectively. The eigenvector pattern of the second EOF is a little more complicated than the first EOF. Positive values are apparent to middle and lower reaches of Yangtze River, the Northeast China and to the north of the Tianshan Mountains, whereas negative values are seen over Taklimakan Desert and South China. The time series show a decadal-scale variability, with negative extreme scores in 1970's.

5.2 The contribution of June, July and August precipitation to the dominants mode of summer precipitation

Though traditional climatological seasons have been used to compare with other results, the seasonal as well as inter-annual atmospheric circulation changes largely in June, July and August around East Asia. To assess the reliability of these two modes (SMR EOFs) and the contribution of each summer month, the anomalies for all the summer months (*i.e.*, 36 × 3 months for each station) are

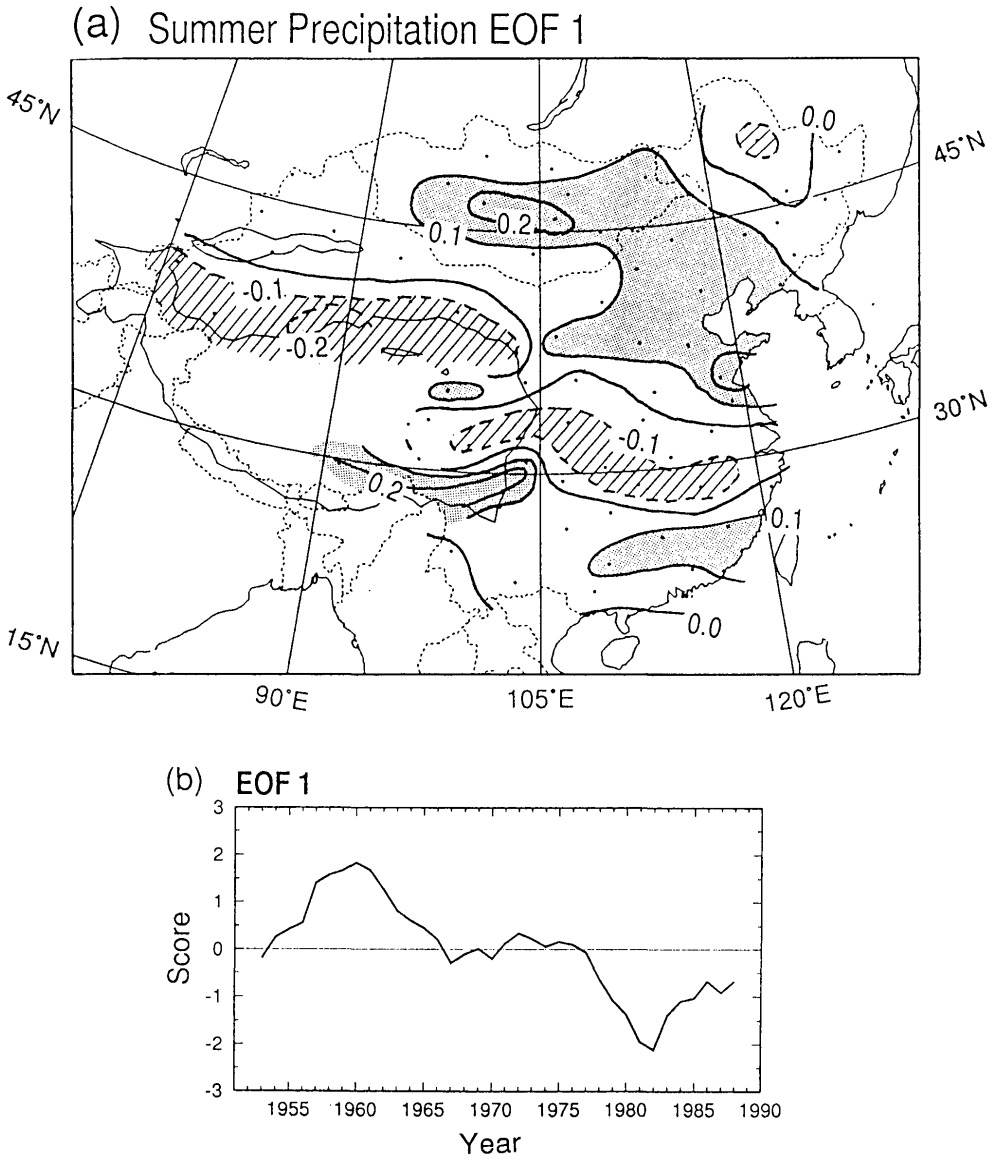

Fig. 7. Eigenvector patterns and time coefficients of the first two EOFs of summer precipitation. (a) The eigenvector pattern of EOF 1. Dots show the 70 stations used for the EOF analysis. The contour interval is 0.1 with negative values dashed. Shaded (hatched) areas indicate eigenvector exceeds (below) 0.1 (−0.1). (b) Scores are standardized. (c) (d) are the same with (a) (b), but for the EOF 2.

subjected to the EOF analysis (S-JJA EOFs).

The identical eigenvector patterns with SMR EOFs were obtained in the first two S-JJA EOFs, but their order is reversed. The variances of the two EOFs are 11.2 % and 10.6 %, respectively. They are relatively small compared to those of SMR EOF, which may be due to the sample size (of 3 times in number) and month-to-month difference in the S-JJA EOF analysis. We could identify that the SMR EOF 1 is fundamentally the same as the S-JJA EOF 2, though the eigenvectors and the scores are reversed in sign. Figure 8 depicts the scores of (a) S-JJA EOF 2 for SMR EOF 1, and (b) S-JJA EOF 1 for SMR EOF 2. In the S-JJA EOF 2 (Fig. 8a), the scores of June and July change nearly synchronously, except in the late 1960s. This figure shows that the variation in July and June contribute mostly to the SMR EOF 1 (the three belt pattern), and the correlation between each score of the S-JJA EOF 2 (June, July and August) and the SMR EOF 1 is −0.88, −0.92 and −0.35, respectively. In the S-JJA EOF 1 (Fig. 8b), on the contrary, the scores of August and July change in phase, but that of June shows a different feature, especially in 1960s and around 1980. The correlation between each score of the S-JJA EOF 1 and the SMR EOF 2 is 0.38, 0.60 and 0.79, respectively. So we may conclude the decadal-scale variations in July and June contribute

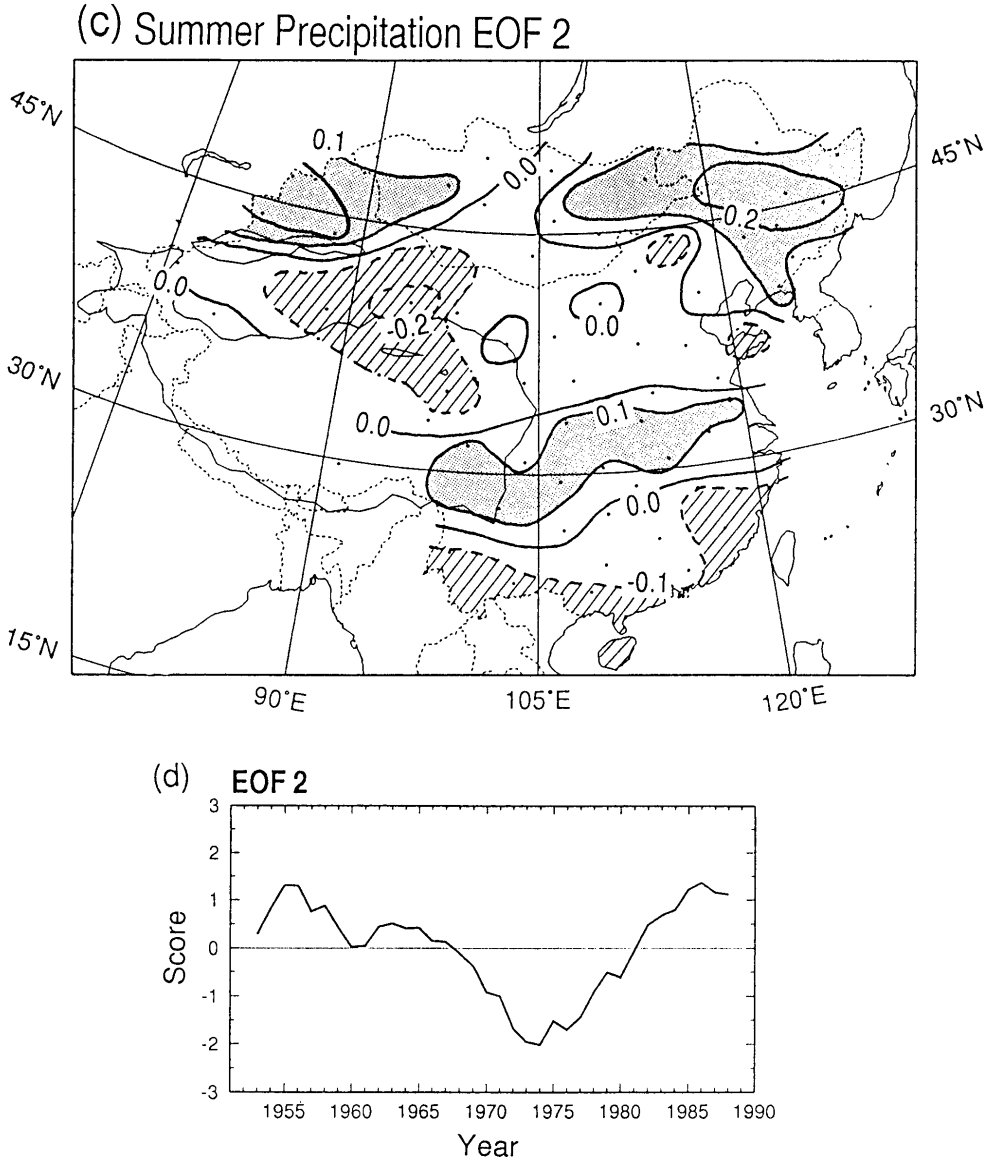

Fig. 7. (Continued)

most to the SMR EOF 1 (Fig. 7b), while August and July contribute most to the SMR EOF 2 (Fig. 7d).

5.3 Relationship to temperature change over China and NHT in summer

To examine the relationship between the dominant EOFs of summer temperature and simultaneous precipitation, the EOF analysis is also applied to the mean summer temperature, as shown in Fig. 9. The first and second EOF share 30.0 % and 18.6 % of the total variance, respectively, which is larger than that of precipitation (Table 3). The first two modes of summer temperatures (Fig. 9a, 9c) show similar patterns to those of precipitation (Fig. 7a, 7c), but with reversed signs of eigenvectors. Furthermore, the scores of each component (thick line) shows simultaneous variation with that of precipitation (shown in Fig. 7b, 7d in dashed line) in the same sign. These results imply that there are strong negative correlations between the temperature and precipitation, both in the first two components. The correlation coefficients between temperature and precipitation scores are 0.87 for EOF 1 and 0.60 for EOF 2, respectively.

The pattern of the first EOFs in temperature is also very similar to that of the linear trend (Fig. 2d). The score (Fig. 9b) shows a decreasing trend, which means Central China and Taklimakan Desert have been cooling, and so on.

The correlation between the second component of temperature and precipitation in summer is 0.60, which is not so high as that of the first component (0.87). This was caused by the different score from the late 1950s to early 1960s. The eigenvector pattern of the second component of tempera-

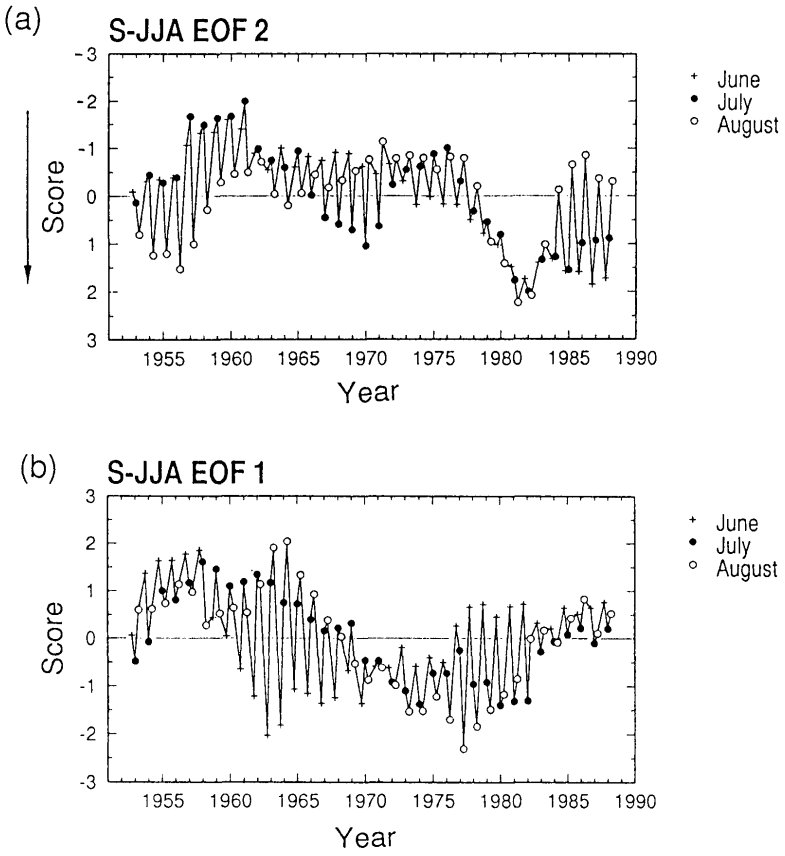

Fig. 8. Scores of the S-JJA EOFs (a) for the second component and (b) the first component. In (a) the Y-axis is upside-down to compare with the score of the SMR EOF 1 (Fig. 7b). (b) corresponds to Fig. 7d. The crosses indicates June, and black and white circles mean July and August, respectively.

ture (Fig. 9c) resembles, as a whole, that of precipitation (Fig. 7c). The NHT in summer changes simultaneously with the second score of temperature EOF. Hence this mode explains the strong relationship with NHT, and most part of China have positive eigenvectors. The correlation pattern between NHT and summer temperature of each station (not shown) are very similar to Fig. 9c. Namely, large strong positive correlation spreads over South, Southwest and Northeast China, whereas some stations in Northwest China show negative high correlation with NHT as seen in Fig. 9c. The correlation coefficient between NHT and EOF 2 in temperature and precipitation is 0.85 and 0.75, respectively.

The correlation coefficient between EOF 2 of summer temperature and NHT is very high, while the leading mode of winter temperature does not show a strong correlation with NHT as discussed in subsection 4.3. Wallace *et al.* (1993) showed the leading EOF of wintertime 500 hPa height is closely related to the PNA pattern while the summertime and annual-mean 500 hPa height and thickness are of the same polarity throughout almost the entire hemisphere. They attributed the notable exception in wintertime global circulation to the fact that the PNA pattern and other regional teleconnection patterns are strongest in winter. The first two modes of winter temperature deduced in section 4 were associated with dynamical variability related to the PNA and some other teleconnection patterns. So our result supports their idea; the relatively weak correlation between the EOF 1 of winter temperature and NHT was caused by the strong regional teleconnections, while the strong correlation between the EOF 2 of summer temperature and NHT was reflected by the same polarity throughout almost the entire hemisphere.

5.4 Atmospheric circulation patterns associated with summer precipitation and temperature EOFs

Figure 10 shows the correlation pattern between the EOF 1 of summer precipitation and (a) the 500 hPa height and (b) SLP anomalies. At the 500 hPa height (Fig. 10a), a large elongated negative belt is apparent over the Eurasian Continent centered over the Caspian Sea, which implies that when relatively less precipitation occurs in the Central China to Taklimakan (refer to Fig. 7a), the height of this elongated area is lower, and is higher to the south of it (the area from southwest of Tibetan

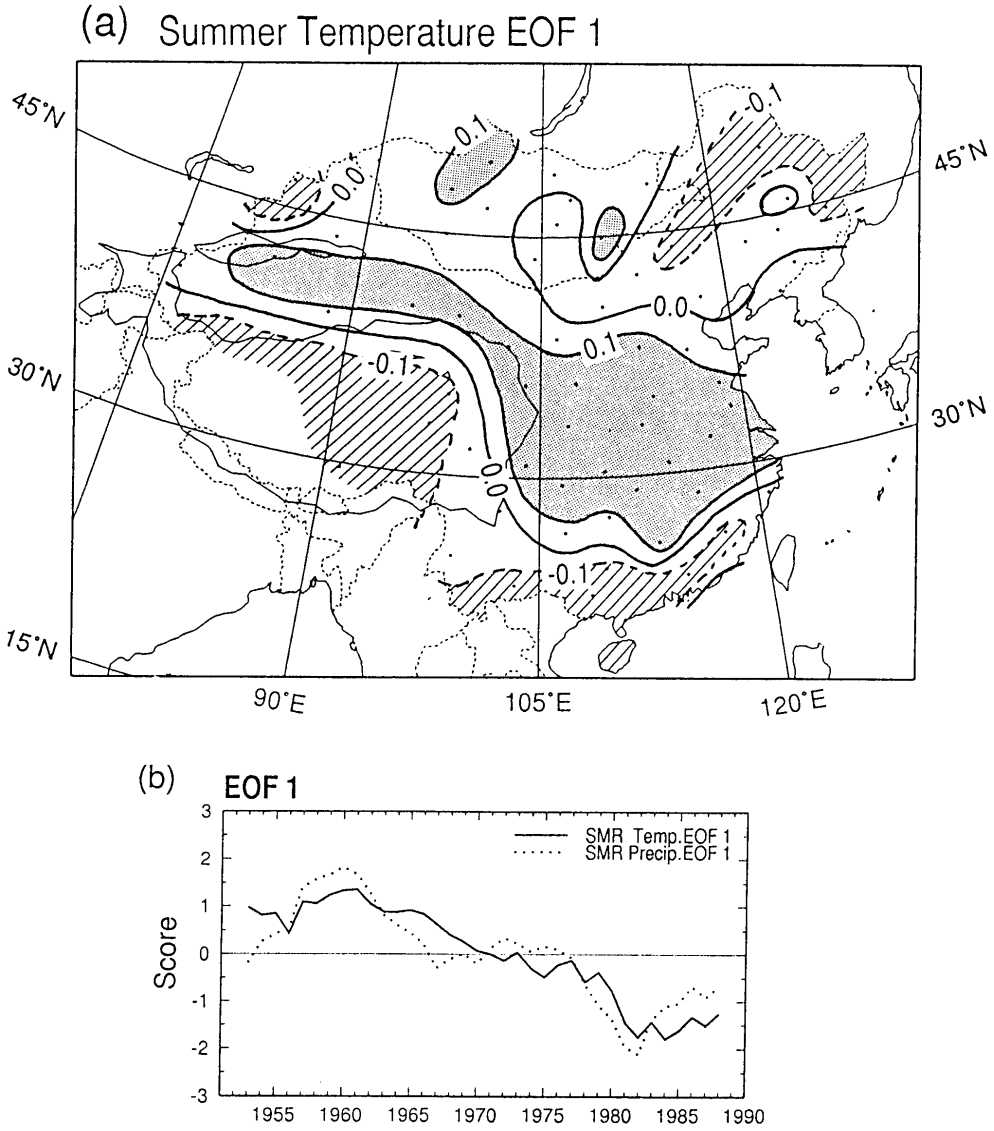

Fig. 9. Eigenvector patterns and time coefficients of the first two EOFs of summer temperature. (a) (b) for the 1st component, and (c) (d) for the 2nd component. Details are the same as for Fig. 7. The dotted line in (b) (d) denotes the corresponding the score of summer precipitation EOFs, namely the dotted line in (b) is same as in Fig. 7b and in (d) as in Fig. 7d. The thin line in (d) is NHT summer, which appeared in Fig. 5.

Plateau to Northwest China). In this situation, the zonal wind should be more strong. In the corresponding SLP correlation (Fig. 10b), a strong negative correlation is noted over central Asia, which corresponds to the negative center of the 500 hPa height. This correlation may be related to the advance (or retreat) of the trough over central Asia. Over China, a strong negative correlation indicates westward extension of Pacific High. Namely, when less precipitation is seen over Central China and Taklimakan Desert, the Pacific High comes more westward.

The correlation pattern between the EOF 2 and the 500 hPa and SLP anomalies are mapped in Figs. 10c and 10d, respectively. High positive correlations are seen over the northeastern Pacific and the Mediterranean Sea, and significant negative correlations are located over the northwestern Atlantic, both in the 500 hPa and SLP fields. A positive correlation exists over the north of India only in the 500 hPa height pattern, though it is not so significant as that in SLP field. Interestingly, this component roughly shows a wave-one type pattern in 30°N–60°N with negative values over and around the north Atlantic Ocean through Europe and positive values over Eurasia through the northwest of North America both in the SLP field. The correlation fields between NHT in summer and the 500 hPa

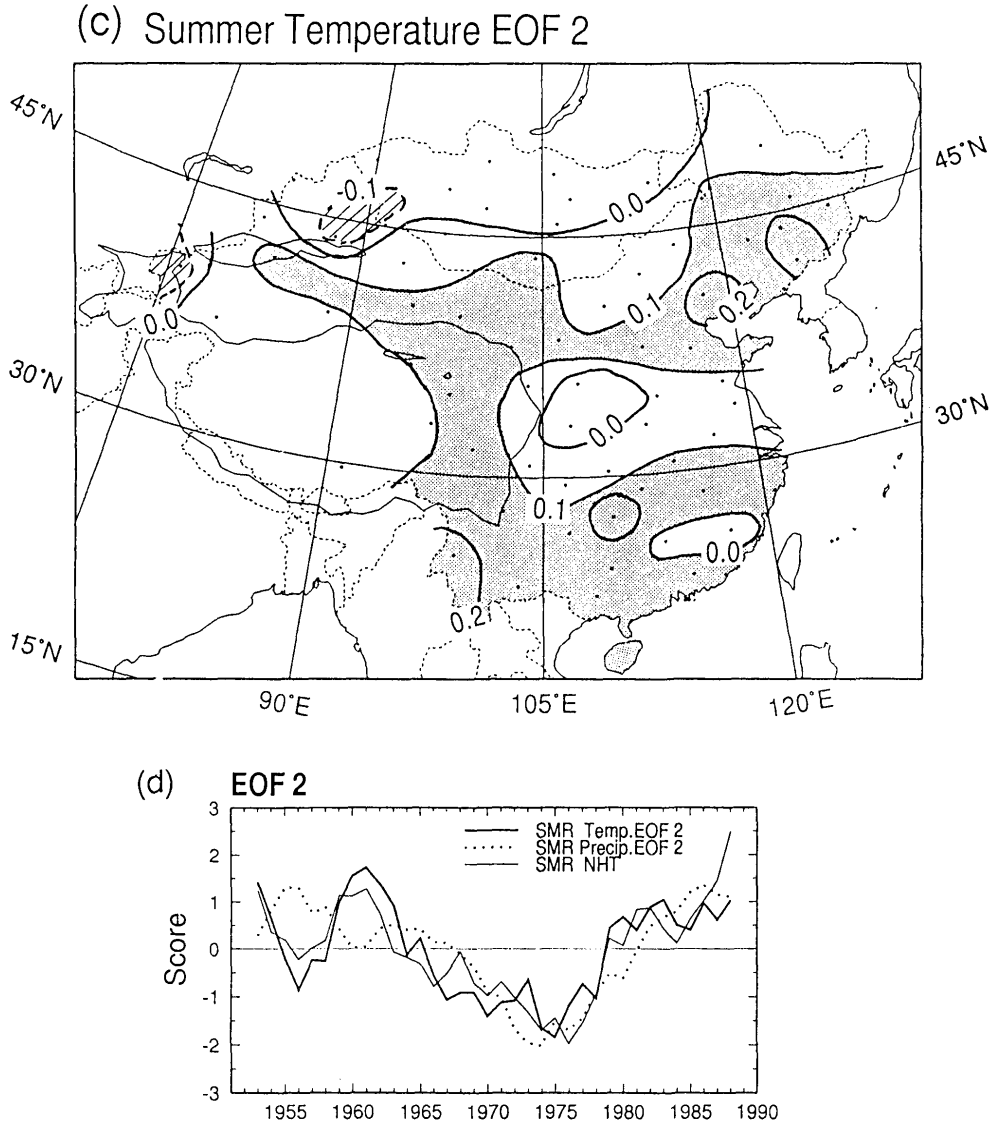

Fig. 9. (Continued)

and SLP anomaly are identical with that of Figs. 10c and 10d, but the correlation over the Pacific are more strong in both the 500 hPa and SLP fields than Figs. 10c and 10d.

As discussed in Subsection 5.2, the circulation field in summer changes from June to August. The correlation distribution between S-JJA scores, and each month the 500 hPa and SLP anomaly are also examined (not shown). The second component of the S-JJA (related to three-belt SMR EOF 1) is mostly influenced by July and June. Thus the correlation field with July score resembles Figs. 10a and 10b very well, and the correlation of June is also similar to them but it has strong positive correlation over the Pacific Ocean. On the other hand, Fig. 10b resembles that of the August and July of the first component of the S-JJA (related to NHT, SMR EOF 2).

Table 3. The variances and cumulative variances of the first five EOFs of summer temperature.

Component	1	2	3	4	5
Variance (%)	30.0	18.6	13.2	11.5	6.4
Cumulative Variance (%)	30.0	48.6	61.8	73.3	79.7

6. Conclusions and remarks

We have presented the linear trends and decadal-scale fluctuations in temperature and precipitation in China and Mongolia for the recent 40-year period, along with their associations with the hemispheric atmospheric circulation patterns and the NHT.

The apparent warming trend of the annual mean

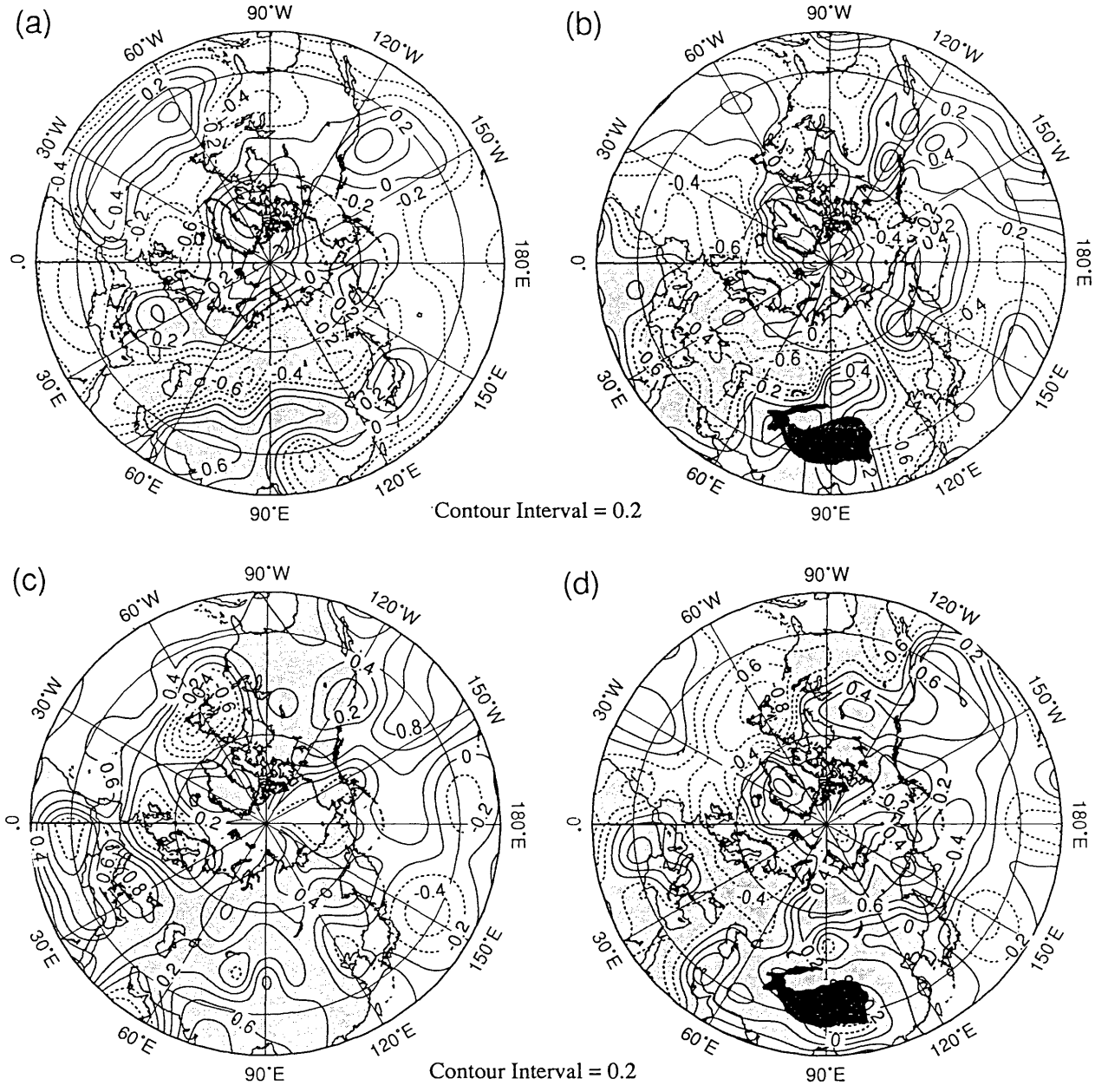

Fig. 10. The correlation coefficients between time coefficient of the first two EOFs of summer precipitation. Details are the same as for Fig. 5.

temperature was identified in North, Northeast Northwest China and Mongolia, while a cooling trend was seen just to the east of the Tibetan Plateau (Southwest China). The annual mean warming trend is remarkable in the northern part of China, which is considered to be a part of the hemispheric warming pattern (*e.g.*, IPCC, 1990; Jones and Briffa, 1992). The winter and spring temperature trends contribute a great deal to the annual temperature trends. In summer, a large decreasing trend is seen over Central China and Taklimakan Desert.

By applying EOF analysis to winter temperature to examine the time-space structure of decadal-scale variation, two notable patterns were obtained. The first pattern was the decadal-scale oscillation in the same sign over the whole of China, except the Tibetan Plateau and Southwest China. This mode is related to decadal-scale change of the hemispheric circulation, involving the pressure change over Eurasian continent and the PNA pattern. The second spatial pattern resembles the linear trend pattern over China and Mongolia, with warming in the northern part and cooling in the southern part of study area. This mode is basically associated with the circulation over central and eastern part

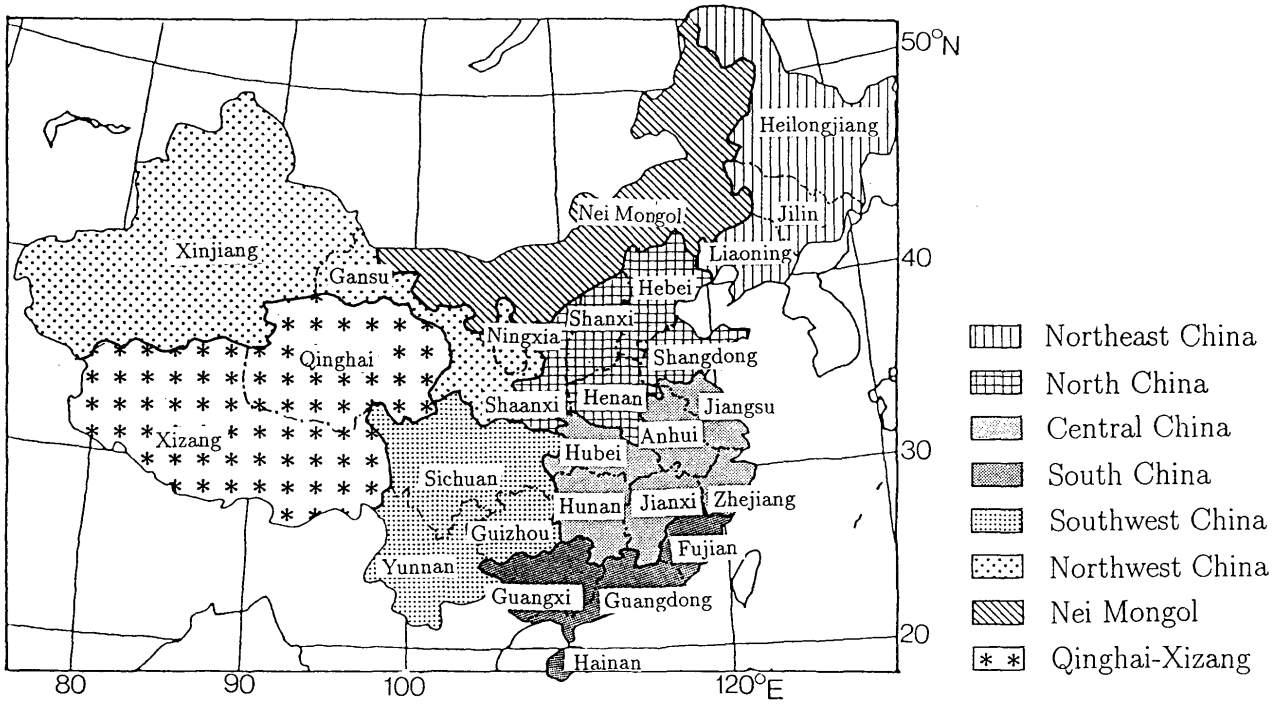

Fig. A1. China's present administrative units and traditional divisions.

of Eurasia and Pacific sector. These two modes of winter temperature over China seem to be closely related to the changes of the patterns of cold surge from Siberia, as Yasunari and Tian (1990) have suggested.

The linear and decadal-scale variation in summer precipitation, which comprises the most part of the annual precipitation, was related to that of temperature variation in the same season. The linear trend and the EOF 1 mode exhibits increasing precipitation over Taklimakan to Yangtze River reaches, and decreasing precipitation over Mongolia, Nei Mongolia, North, South and Southwest China. The July and June precipitation contributes strongly to this summer (JJA) EOF 1. This three-belt pattern is also shown in the first EOF of summer temperature, but reversed in sign. This mode seems to be related to the changes in atmospheric circulation anomaly over the Eurasian continent and the extent of the Pacific high pressure.

On the other hand, the second EOF pattern of summer precipitation shows strong positive areas extending to the Northeast and Central China and to the north of Tianshan Mountains, whereas the negative area exists in South China and Taklimakan. The summer precipitation EOF 2 is affected by the variation in August and July. This mode is related to the NHT in summer and the hemispheric wave-one type anomaly in the higher latitudes.

These results suggest the importance of regional characteristics in the decadal-scale fluctuation when we deal with the global warming issue. It is noteworthy to state that the correlation is preferentially significant between the summertime (not wintertime) NHT and the second EOFs of summer temperature and precipitation over China and Mongolia, which implies that the association between the recent hemispheric (wintertime) warming and the climate change over east Asia is not straightforward. In order to validate the relation between the regional and global climate changes, analyses based upon a more uniformly and densely distributed global data set, including the satellite information, will be essential.

Acknowledgments

The authors would like to thank Dr. P.D. Jones, Univ. of East Anglia for releasing us the NHT data. Prof. T. Mikami, Tokyo Metropolitan University kindly supplied us a copy of the data set. We thank Dr. Tsohiogyn Adyasuren, Ministry for Nature and Environment of Mongolia for providing the temperature and precipitation data over Mongolia. We would like to offer appreciation Dr. R. Kawamura, National Research Institute for Earth Science and Disaster Prevention, for fruitful discussion and useful comment. The two anonymous reviewers' comments were helpful in the revision of this paper. We also thank Mr. Tian Shao-Fen, for advising and guiding the computer processing. Part of this work was supported by the research fund for science promotion from Science and Technology Agency, and by the subsidy for scientific research from Chubu Electric Power Co., Inc.

Appendix

China's present administrative units and traditional divisions

There are now 30 first-level administrative units in China including 3 of municipalities (Beijing, Tianjin and Shanghai).

Figure A1 is drawn up on referring to Domrös and Peng (1988) and the Atlas of Physical Geography of China (1984). It shows the 27 provinces or autonomous regions, and traditional divisions with hatching, dots, *etc.* The eight divisions used in this study are; Northeast China (Beidon, in Chinese), North China (Hua bei), Central China (Hua zhong), South China (Hua nan), Southwest China (Nanxi), Northwest China (Xibei), Nei Mongol (Nei menggu) and Qinghai-Xizang (Qingzang).

References

Barnston, A.G. and R.E. Livezey, 1987: Classification, Seasonality and persistence of low-frequency atmospheric circulation patterns. *Mon. Wea. Rev.*, **115**, 1083–1126.

Bradley, R.S., H.F. Diaz, P.D. Jones and P.M. Kelly, 1987: Secular fluctuations of temperature over Northern Hemisphere land areas and mainland China since the mid-19th century. *The Climate of China and Global Climate*, Y. Duzheng, F. Congbin, C. Jiping, and M. Yoshino, Eds., China Press and Springer Verlag, 76–87.

Chen, L.-X., M. Dong and Y.-N. Shao, 1992: The characteristics of interannual variations of the East Asian Monsoon. *J. Meteor. Soc. Japan*, **70**, 397–421.

Chen, L.-X., Y.-N. Shao, M. Dong, Z.-H. Ren and G.-S. Tian, 1991: Preliminary analysis of climate variation during the last 39 years in China. *Adv. Atmos. Sci.*, **8**, 279–288.

Diaz, H.F., R.S. Bradley and J.K. Eischeid, 1989: Precipitations fluctuations over global land areas since the late 1800's. *J. Geophys. Res.*, **94**, No. D1, 1195–1210.

Domrös, M. and G. Peng, 1988: *The Climate of China*, Springer-Verlag, 360 pp.

Huang, J.Y., 1991: Analysis of temporal and spatial characteristics for temperature and precipitation in summer of China. *Sci. Atmos. Sinica*, **15**, 124–132 (in Chinese with English abstract).

Huang, R.H., 1992: WCRP in China and its results. *Tenki*, **39**, 541–550 (in Japanese).

IPCC, 1990: *Climate Change: The IPCC scientific assessment.* J.T. Houghton, G.J. Jenkins and J. Ephraums, (Eds.). Cambridge University Press, Cambridge, UK, 365 pp.

IPCC, 1992: *Climate Change 1992: The supplementary report to the IPCC scientific assessment.* J.T. Houghton, B.A. Callander and S.K.Varney, (Eds.). Cambridge University Press, Cambridge, UK, 200 pp.

Jones, P.D., R.S. Bradley, H.F. Diaz, P.M. Kelly and T.M.L. Wigley, 1986: Northern Hemisphere surface air temperature variations: 1851–1984. *J. Climate Appl. Meteor.*, **25**, 161–179.

Jones, P.D. and K.R. Briffa, 1992: Global surface air temperature variations during the twentieth century: Part 1, spatial, temporal and seasonal details. *Holocene*, **2**, 2, 165–179.

Kashiwabara, T., 1987: On the recent winter cooling in the North Pacific. *Tenki*, **34**, 777–781 (in Japanese).

Li, K.-R., X.-C. Lin and W.-C. Wang, 1990: The long-range variational trend of temperature in China from 1951 to 1988. *Geogr. Res.*, **9(4)**, 26–37 (in Chinese with English abstract).

Nitta, T., and S. Yamada, 1989: Recent warming of tropical sea surface temperature and its relationship to the Northern-Hemisphere circulation. *J. Meteor. Soc. Japan*, **67**, 375–383.

Nitta, T. and J. Yoshimura, 1993: Trends and interannual and interdecadal variations of global land surface air temperature. *J. Meteor. Soc. Japan*, **71**, 367–375.

The map publisher of China, 1984: *Atlas of physical geography of China* (in Chinese).

Tian, S.-F. and T. Yasunari, 1992: Time and space structure of inter-annual variations in summer rainfall over China. *J. Meteor. Soc. Japan*, **70**, 585–596.

Trenberth, K.E., 1990: Recent observed interdecadal climate changes in the Northern Hemisphere. *Bull. Amer. Meteor. Soc.*, **71**, 988–993.

Wallace, J.M. and D.S. Gutzler, 1981: Teleconnections in the geopotential height field during the Northern Hemisphere winter. *Mon. Wea. Rev.*, **109**, 784–812.

Wallace, J.M., Y. Zhang and K.-H. Lau, 1993: Structure and seasonality of interannual and interdecadal variability of the geopotential height and temperature fields in the Northern Hemisphere troposphere. *J. Climate*, **6**, 2063–2082.

Wang, P.K. and D. Zhang, 1992: Recent studies of the reconstruction of East Asian monsoon climate in the past using historical literature of China. *J. Meteor. Soc. Japan*, **70**, 423–446.

Wang, S.-W. and Z.-C. Zhao, 1981: Droughts and floods in China, 1470–1979. *Climate and History*, Wigley, Ingram, and Farmer, Eds., Cambridge, 271–288.

Yasunari, T. and Y. Seki, 1992: Role of the Asian Monsoon on the interannual variability of the global climate system. *J. Meteor. Soc. Japan*, **70**, 177–189.

Yasunari, T. and S.-F. Tian, 1990: Large-scale atmospheric Circulation Patterns Associated with the cold surges in Yunnan Province,China. *Geogr. Rev. Japan*, **62B**, 161–169.

Yoshino, M.M. and M. Chiba, 1984: Regonal division of China by precipitation and its annual variation type. *Geogr. Rev. Japan*, **57A**, 583–590.

中国とモンゴルにおける最近40年間 (1951–1990) の地上気温と降水量のトレンドと10年スケールの変動

谷田貝亜紀代
(筑波大学地球科学研究科)
安成哲三
(筑波大学地球科学系)

中国とモンゴルにおける気温と降水量の線形トレンドと10年スケールの変動の時空間構造を、1951年–1990年の5年移動平均した時系列を用いて調べた。主成分分析 (EOF 解析) の手法を季節平均気温、降水量に適用した。これらの変動に伴う大気循環場の変動を500 hPa等圧面高度と地上気圧場の偏差を用いて解析した。また、北半球平均地上気温データとの相関も調べた。主な結果は次のように要約される。

年平均気温はモンゴル、中国華北・東北・西北地方で顕著な昇温傾向が見られ、四川省～雲南省 (中国西南部) での降温傾向がみられた。この傾向は主に冬季と春季の偏差によっている。冬季の気温のEOF解析の結果、チベット高原を除く対象地域全体で同符号の偏差を表すモードが卓越し (寄与率51.3 %)、時系列は10年スケールの周期的変動を示した。このモードは、ユーラシア大陸のシベリア高気圧の強さ、偏西風の強さに密接に関係し、PNAパターンや大西洋の高度偏差とも相関が見られた。一方第2主成分は、対象地域の南北の逆符号の空間パターンを示し、1950年代前半の北 (南) 部の低 (高) 温と1980年代の北 (南) 部の高 (低) 温をあらわしている。この成分は、寒気がチベット高原の北、東縁を南下するモードに関係し、北太平洋の高度偏差と関連していた。

年降水量は、中国の最南部が顕著な増加傾向、華北、華南の減少傾向のほかは、ほとんど有意なトレンドは得られなかった。対象地域で年降水量のほとんどを占める夏季降水量のEOF解析の卓越成分は、夏季気温の主成分と相関が見られた。第1主成分は、モンゴルから華北で正 (負)、タクラマカンから華中で負 (正)、西南、華南で正 (負) という空間分布をしており、スコアは減少傾向が見られた。この成分は、7, 6月の寄与が強く、ユーラシア大陸上の循環場の偏差と対応が見られた。一方、第2主成分は、天山山脈の北側と東北、華中で正、タクラマカンと華南で負という複雑な空間パターンを呈したが、時系列は北半球平均気温と密接に関係していた。またこのモードには8, 7月の寄与が高かった。